Journal of the European Ceramic Society 35 (2015) 3587–3594

Contents lists available at www.sciencedirect.com

Journal of the European Ceramic Society

journal homepage: www.elsevier.com/locate/jeurceramsoc

Design and fabrication of ceramic beads by the vibration method

Christian J. Espinoza Santos[a], Arif Z. Nelson[b], Elena Mendoza[c], Randy H. Ewoldt[b], Waltraud M. Kriven[a,*]

[a] Department of Materials Science and Engineering, the University of Illinois at Urbana-Champaign, Champaign, IL, United States
[b] Department of Mechanical Science and Engineering, the University of Illinois at Urbana-Champaign, Champaign, IL, United States
[c] Department of Chemical and Biomolecular Engineering, the University of Illinois at Urbana-Champaign, Champaign, IL, United States

ARTICLE INFO

Article history:
Received 17 November 2014
Received in revised form 12 May 2015
Accepted 14 May 2015
Available online 17 June 2015

Keywords:
Viscoelastic solid
Alumina paste
Vibration method
Alumina beads

ABSTRACT

The purpose of this of study was to investigate the confined vibration method to produce alumina beads for the study of stress wave propagation in granular media. The method produces beads with desirable shape (i.e. oblate, prolate, and tri-axial ellipsoid), microstructure (level of porosity), and size (5 mm to 3 cm in diameter). This environmentally friendly approach to process beads involves preparing a slurry with a small amount of PVA binder and dispersant. After drying, the pre-formed material is a shear-reversible soft-solid, which flows under applied stress with limited strain recovery. This rheological behavior is sufficient for the alumina paste to be processed into rounded shapes with a confined shaker table and to maintain the shape for sintering of the alumina beads.

1. Introduction

Early work by Hertz [1] to understand the contact interaction between granular media motivated a series of publications [2–4] focusing on theoretical and numerical predictions. The problem was extended to 1D granular chains to observe the formation of solitary waves and it was found that solitary waves occur when five or more beads are in contact [5,6]. While, some experimental work [7,8] was conducted to understand stress wave propagation in granular media, a limitation [9] to further the research was due to the limited amount of choices in terms of bead size and bead composition.

In terms of bead size, forming methods such as single and multiple needle systems [10–12], rotating atomizer for viscous liquids [13], perforated plates [14], a nozzle mounted in a rotated cylinder [15,16], rotating disc atomization [17] and electrostatic dripping [18–20] have been used to make ceramic beads. However, these methods only produce beads with diameters below 5 mm [12,21–27].

This motivated our team to design a new processing technique to make ceramic beads using a modified version of the vibration molding method. The colloidal vibration molding method was previously introduced by Franks et al. [28] where it was demonstrated that saturated ceramic paste, consolidated by either centrifugation or pressure filtration, could be fluidized by vibration and made to flow into a die to produce complex green body shapes [28–31]. Though this approach was successful in producing complex shapes, information about producing spherical beads using this technique has not been reported in the current literature [28,32–34]. A modified version of the colloidal vibration molding method was introduced by our labs to produce ceramic beads ranging from 0.5 mm to 3 cm in diameter. During an attempted slip casting using a plaster of Paris mold [35,36], it was observed that small drops of solution had dripped directly onto the vibrating table being used to vibrate the alumina mixture into the mold. When this occurred, the small drops of alumina solution formed themselves into small spheres.

The vibration kept the material sufficiently soft enough to deform and hard enough to cause the spheres to bounce around randomly, helping to round them out. As the beads slowly dried, they retained their spherical shape. In an effort to improve the quality and reproducibility of alumina beads, processing parameters were optimized for the original forming process. This work demonstrates how different parameters such as the slurry formulation and processing variables of paste rheology affect the formation of the alumina beads. More specifically, this work focuses on:

1.1 Optimizing the alumina slurry formulation by changing the amount of binder.
1.2 Evaluating the rheological behavior of the paste to understand the bead shape evolution from non-spherical to spherical.

* Corresponding author. Tel.: +1 217 333 5258; fax: +1 217 333 2736.
E-mail address: kriven@illinois.edu (W.M. Kriven).

http://dx.doi.org/10.1016/j.jeurceramsoc.2015.05.018
0955-2219/

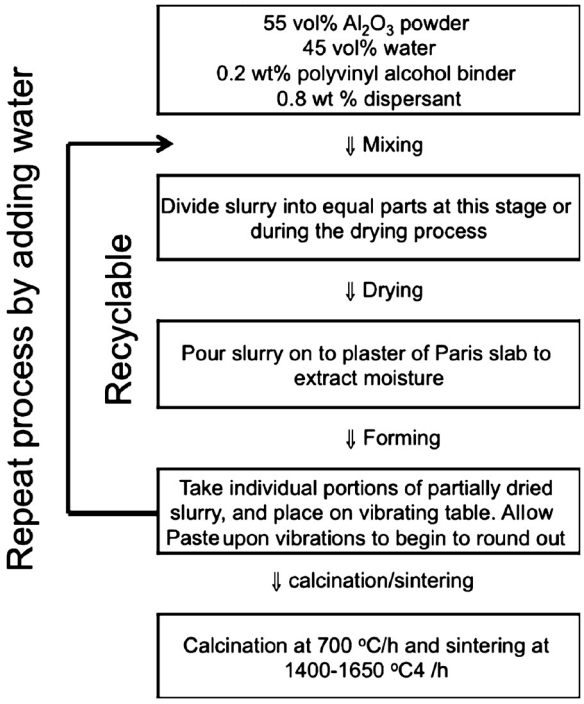

Fig. 1. Bead forming process showing the four main steps (mixing, drying, forming, and calcination/sintering) to make alumina beads.

1.3 Standardizing the vibration process to make beads reproducibly.
1.4 Evaluating the performance of the alumina beads in terms of breaking force and number of rotating cycles.

2. Experimental procedures

The experimental procedure to make alumina beads involves four main steps: preparation of the slurry, drying of the slurry, formation of the paste, and calcination/sintering of the beads as shown in Fig. 1.

2.1. Materials

The experimental procedure to make ceramic beads started with the procurement of alumina powder (A 152 SG Almatis Premium Alumina, Bauxite, AR) with particle size of 1.2 μm and surface area 4.3 m^2/g, polyvinyl alcohol (PVA) binder, 80% hydrolyzed with MW = 9000–10,000, (PVA binder, Sigma-Aldrich, Saint Louis, MO), and D-3005 dispersant of MW ~ 2400 (Rohm and Haas, Philadelphia, PA).

2.2. Preparation of alumina paste

An alumina slurry was prepared in two steps. First, 55 vol% (82 wt%) of alumina powder was dispersed in 45 vol% (17.3 wt%) distilled water using a 0.8 wt% of ammonium salt dispersant (Duramax 3005) and was mixed for 15 min with a magnetic stirrer. All of the additives in the suspension, which included the dispersant and binder, were measured as a function of wt% alumina added. Second, 0.1, 0.3, and 0.5 wt% of PVA binder was added to the alumina suspension using a magnetic stir plate at room temperature for a period of 30 min, or until all of the binder was fully dissolved in the suspension. The prepared slurry was poured onto a slip-casting platform for partial dehydration before forming. The partial dehydration process of the alumina slurry created alumina paste with ~9 wt% water content. Table 1 shows an example of the slurry formulation before and after dehydration. It is important to clarify that after partial removal of the water, the alumina slurry become a paste. The moisture in the alumina slurry was measured by recording the weight before and after the slurries were poured onto the slip-casting platform.

2.3. Rheology of the alumina slurry

The rheological behavior of the suspensions was analyzed to gain an insight into the slurry characteristics, which eventually helped to obtain reproducible, consistent behavior. The rheological behavior of the suspensions was measured with a controlled stress (CS) rheometer (CS10, Bohlin Gemini, Worcestershire, UK), in which the apparent viscosity was measured as a function of shear rate. The controlled stress rheometer was fitted in a concentric cylindrical geometry (CS 25, Bohlin Gemini, Worcestershire, UK).

2.4. Rheology of the alumina paste

The rheological behavior of the alumina paste was analyzed to evaluate the material response and to gain a better understanding of the bead forming evolution. In order to probe the viscoelastic properties, alumina paste samples were subjected to simple shear deformation with an AR-G2 rotational rheometer (TA Instruments, New Castle, DE). A 40 mm diameter, parallel plate geometry was used for all testing. All stresses reported were apparent stress from direct mapping to the total torque. Temperature was controlled at 25 °C via a Peltier plate. Adhesive-backed 600 grit sandpaper was attached to the parallel plate and Peltier plate to minimize slip. With sandpaper attached, steady shear viscosity measurements at different gaps were in agreement (the difference between 1000 and 800 μm gaps were within the precision error of reproducibility tests at 1000 μm), thus indicating that slip was not significant.

The alumina paste was poured onto the bottom plate and the top plate was lowered to make contact with the sample. The top plate was then slowly lowered while being slowly rotated by hand so that the sample would completely fill the gap. The sample was trimmed with a spatula around the end of the plate for proper filling. A solvent trap with distilled water was loaded over the top plate to prevent evaporation from the sample. For consistent results, samples were subjected to a prescribed deformation history after loading and before rheological characterization: A shear stress of 100 Pa was applied for 120 s, then removed for 30 s to reset the deformation history.

To identify the range of strains for which a linear viscoelastic response would be observed, an oscillatory strain amplitude sweep was performed at the highest frequency to be tested. The subsequent frequency sweeps were then performed at a strain which fell within the linear viscoelastic regime of the initial strain sweep. Shear creep and recovery experiments were also performed using the same experimental setup to determine the steady state viscosity as well as the recovery response. After the loading procedure, a particular shear stress was applied for 120 s after which the strain recovery was recorded for 30 s.

2.5. Fabrication of spherical green bodies

The alumina paste was placed on the vibrating table and a series of dividers were used to contain individual pastes to keep them from sticking together and also to make a large quantity of beads simultaneously (Fig. 2). The divider matrix was moved in a circular motion throughout the process until the spheres were firm enough to hold their shape. The beads were rolled around on the vibrating table for about 5 min, or until they achieved handling strength.

Table 1
An example of the alumina formulation before and after dehydration.

Component	Alumina powder	Dispersant (Duramax 3005)	DI water	Binder (PVA 80% hydrolyzed)
Alumina slurry (before dehydration)*	55 vol% (82.7 wt%)	0.8 wt% (of alumina)	45 vol% 17.3 wt%	0.2 wt% (of alumina)
Alumina paste (after dehydration)**	91.5 wt%	0.8 wt% (of alumina)	8.5 wt%	0.2 wt% (of alumina)

Percentages of the alumina slurry* and paste** are not the same because water is removed from slurry using a porous medium.

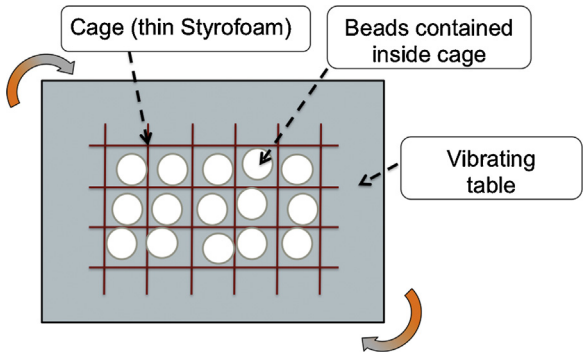

Fig. 2. Experimental setup to make alumina beads.

2.6. Calcination and sintering

Calcination (thermal treatment process) was conducted on the green bodies (beads) to remove the unwanted organic materials that were introduced during the forming process of the beads. Thermogravimetric analysis (TGA) using a Netzsch STA 409 CD (Netzsch Instruments, Selb, Germany) was conducted to observe the water evolution and decomposition of the organic materials during the calcination stage. These studies were conducted at a temperature ranging from 25 °C to 800 °C at 10 °C/min for heating and cooling. As a result, calcination was conducted at 700 °C for 1 h with heating of 0.5 °C/min and cooling down of 5 °C/min because lower heating and cooling rates helped with avoiding thermal shock during the thermal treatment process.

Sintering was conducted to fuse the particles and create a solid ceramic body [37]. During the process, the atoms in the material diffused across the grain boundary of the particles [37]. Sintering in the alumina beads was conducted at temperatures ranging from 1400 °C to 1650 °C for 4 h. A constant time with increasing temperature during sintering was selected to optimize the sintering process of the beads and to observe the changes in density and microstructure evolution. Optimal sintering conditions such as the ones that will be discussed in this paper can enhance properties in the alumina beads resulting in higher density and strength [37].

2.7. Characterization of the alumina beads

The density, breaking force, and number of rotating cycles with microstructure analysis were used to analyze the mechanical properties and performance of the beads. First, the density of each sample was measured following the Archimedes method [38]. In addition, the microstructure of the ceramic beads was observed to confirm the density measurements. Images were taken with a scanning electron microscope (JSM-6060LV, JEOL USA, Inc., Peabody, MA) using excitation energy of 20 kV. Prior to imaging, the samples were Au–Pd sputter-coated for 25 s to prevent charging of specimens. Moreover, the breaking force of the alumina beads was measured on a universal testing machine (Model 4502, Instron Corp., Canton, Mass.). A total of 5 beads per sample condition were analyzed under compression.

Comminution of the ceramic beads was performed in a tumbler to observe the loss of material and reduction of the bead diameter as the number of rotating cycles was increased. This test provided the mass and diameter wear rate of the sintered alumina beads prepared by the vibration method. Friction between the alumina beads during ball milling causes wear in the material when the beads are rolling and sliding over each other [39,40]. The test was conducted for one month at 220 rpm and a total of 32 sintered beads were measured at different time intervals. The mass wear rate (Ω_t) was evaluated based on linear wear theory, where a gradual consumption process takes place by grinding beads inside a tumbler. The mass wear rate (Ω_t) in the ceramic beads was calculated using the following equation:

$$\Omega_t = \frac{\mathrm{d}(m_b)}{\mathrm{d}(t)} = -k_m A_b \tag{1}$$

where $\frac{\mathrm{d}(m_b)}{\mathrm{d}(t)}$ is the mass wear rate as a function of time, A_b is the exposed ball area, and K_m is the mass rate constant of the bead.

Similarly, the diameter wear rate $\frac{\mathrm{d}(D)}{\mathrm{d}(t)}$ in the ceramic beads was calculated using the following equation:

$$\frac{\mathrm{d}(D)}{\mathrm{d}(t)} = -2\frac{k_m}{\rho_b} = -K_d \tag{2}$$

where ρ_b is the ceramic bead density and K_d is the wear rate constant of the bead.

As a last characterization step, the eccentricity of the ceramic beads was measured. The eccentricity [41] is associated with how much something deviates from being circular. The eccentricity of the ceramic beads was measured in three mutually orthogonal planes *xy*, *xz*, and *yz* using the following equation:

$$\sqrt{1 - \frac{b^2}{a^2}} \tag{3}$$

where *a* and *b* are the radii in any plane of the alumina bead. When the result of Eq. (3) is 0, the plane is circular. However, when the result of Eq. (3) is 1, the plane is an ellipse. The 3D construction of the three planes measured in the *xy*, *xz*, and *yz* give either a perfect sphere or an ellipsoid. Eq. (4) provides the graphical representation of the ellipsoid.

$$\frac{x^2}{a^2} + \frac{y^2}{b^2} + \frac{z^2}{c^2} = 1 \tag{4}$$

Based on Eq. (4), any of the bead geometry types can result: a sphere is when radius $a = b = c$, an oblate ellipsoid is when radius $a = b > c$, a prolate ellipsoid is when radius $a = b < c$, and a tri-axial or scalene ellipsoid is when $a > b > c$.

3. Results and discussion

3.1. Formation of green bodies

One of the advantages of the bead forming method is the ability to recycle the dry material, so this method is environmentally friendly because it requires only a small amount of binder and dispersant. The original formulation previously used for slip casting was modified by changing the amount of binder added to the suspension. To improve the formulation, three different amounts of PVA binder were used: 0.1, 0.2, and 0.5 wt% of PVA. To observe the variation in terms of rheology, viscosity measurements were performed in each suspension. It was observed that by increasing

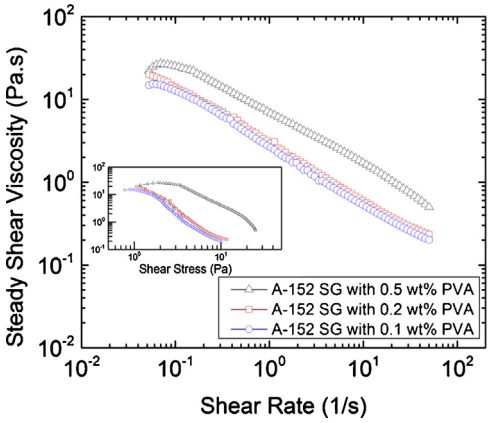

Fig. 3. Viscosity as a function of shear rate of alumina slurries with 0.1, 0.2, and 0.5 wt% polyvinyl alcohol (PVA) binder.

the amount of binder, the viscosity increased as shown in Fig. 3. All three suspensions showed shear thinning behavior for shear stresses above 1 Pa (Fig. 3 inset). The lower PVA concentrations (0.1 and 0.2 wt%) approached a high-rate plateau viscosity for shear stress above 10 Pa.

To test each formulation, all of the alumina slurries went through the same dehydration process (water removal) to form pastes. Through physical observations of the alumina paste when exposed to the vibrating table, the following were determined: (a) with 0.1 wt% PVA binder, the spherical green bodies did not hold their shape well enough; (b) with 0.5 wt% PVA binder, the alumina paste did not flow and the texture of the paste was too sticky; (c) with 0.2 wt% PVA binder, the spherical green bodies retained their shape and had good flowability when the intensity of the vibrating table was increased; (d) the paste that was dried was recycled for new batches. In addition, samples with 0.2 wt% PVA binder were good for making green bodies with a semi smooth surface. Having a smooth surface on the green bodies helped to measure the green body density. The rest of the experiments in this paper were conducted using an alumina paste with 0.2 wt% PVA binder.

3.2. Rheology of the alumina paste

High quality ceramic green (body) beads were formed with the modified vibration molding method with the 0.2 wt% PVA formulation. An important aspect of the research was focused on understanding the type of rheology associated with the ability to form the paste into round shapes with the confined vibration processing method. The first observation while forming the beads was that the alumina paste required flowability under applied stress. Second, the alumina paste needed to be moldable, but with the ability to retain its shape. During rheological measurements of the paste, shear thickening at high stress was observed. Previous literature reported shear thickening in high loading slurries [42]. However, it was unclear whether the formation of green body beads was purely dependent on a specific type of rheological behavior during the formation process. To understand the forming process of the green body beads using the alumina paste, several oscillatory, shear creep and recovery measurements were conducted.

3.3. Oscillatory measurements

During oscillatory measurements, strain amplitude sweeps demonstrated that on time scales of ten seconds or less, alumina paste with 0.2 wt% PVA is a viscoelastic solid with non-linear softening upon the application of large strains or stresses. Fig. 4 shows the results of strain sweeps performed at a frequency of 10 rad/s.

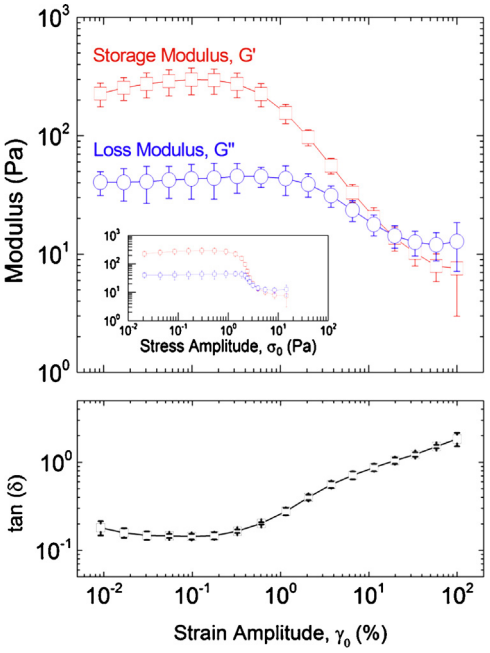

Fig. 4. Strain amplitude sweep of the alumina paste with 0.2 wt% PVA binder at 10 rad/s.

Due to the material's sensitivity to water content, there was much difficulty in obtaining reproducible data. As such, it can be seen that across multiple samples, the linear viscoelastic moduli may vary up to a half order of magnitude. Even with this variability, the qualitative trend clearly shows a linear viscoelastic plateau at low strain (and stress), followed by reversible yielding near an apparent stress amplitude of 2 Pa (Fig. 4 inset).

The results of linear viscoelastic frequency sweeps performed at a strain amplitude of 0.1% can be seen in Fig. 5. Due to the difficulty in obtaining reproducible data across multiple samples, the elastic storage modulus in this case would sometimes vary by over an order of magnitude. However, in the linear viscoelastic

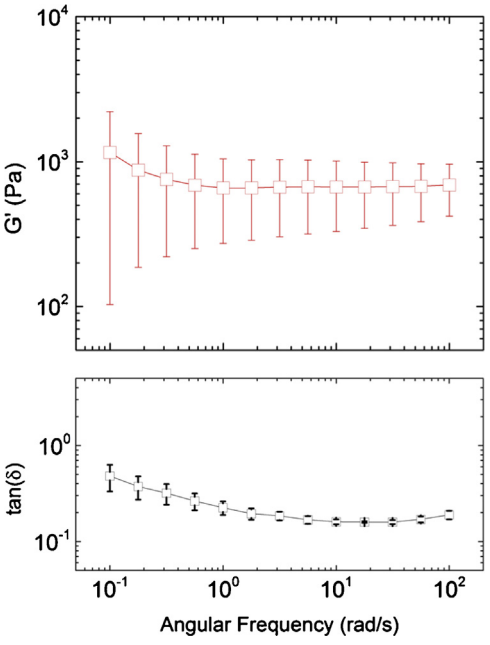

Fig. 5. Linear viscosity frequency sweep of the alumina paste with 0.2 wt% PVA binder at 0.1% strain amplitude.

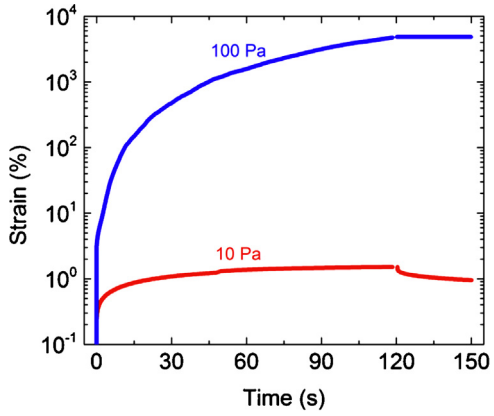

Fig. 6. The nonlinear creep and recovery (after 120 s) of the alumina paste 0.2 wt% PVA binder at 100 Pa and 10 Pa.

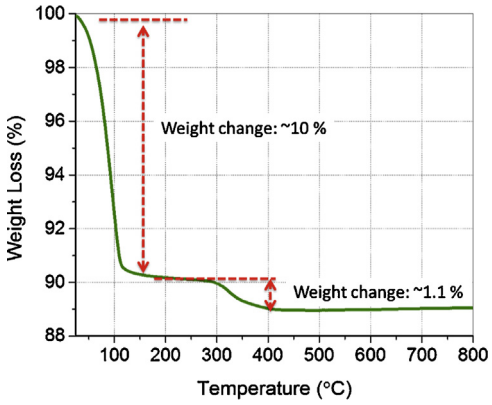

Fig. 8. Thermogravimetric analysis of alumina slurry with 0.2 wt% PVA showing 10% weight loss from 25–100 °C and 1.1% weight loss from. 100–300 °C

regime of small strains, the elastic storage modulus, G', always dominated the viscous loss modulus, G'', as seen by the loss ratio $\tan(\delta) = G''/G'$, the ratio of the viscous loss modulus to the elastic storage modulus, always being less than 1 and as low as 0.2. The sample shows a weak frequency dependence with slightly lower moduli at lower frequencies and slightly higher $\tan(\delta)$ at lower frequencies, but no crossover frequency was observed. During the bead formation process, the frequency of impact was found to be approximately 60 rad/s. This frequency fell within the tested range, indicating that during processing, the material was behaving as a shear-reversible, visco-elasto-plastic solid. The application of large strain amplitudes was limited by instrumental inertia eventually dominating the torque response, but the initial nonlinear response at all tested frequencies universally showed both G' and G'' initially decreasing as a function of applied strain amplitude.

3.4. Shear creep and recovery

The creep and recovery responses of alumina paste containing 0.2 wt% PVA are shown in Fig. 6 for shear stresses of 10 and 100 Pa. Here it can be seen that the nonlinear response was predominantly plastic, as there was little recovery of the accumulated strain. For stresses in the range of 10 to 100 MPa on time scales of the order of 10 s, the maximum recoverable compliance was always less than 1%. Responses within the linear regime could not be verified with creep tests due to poor reproducibility (water evaporation).

The steady state viscosity data for stresses in the range of 10 to 1000 Pa can be seen in Fig. 7. Within this range, shear thickening

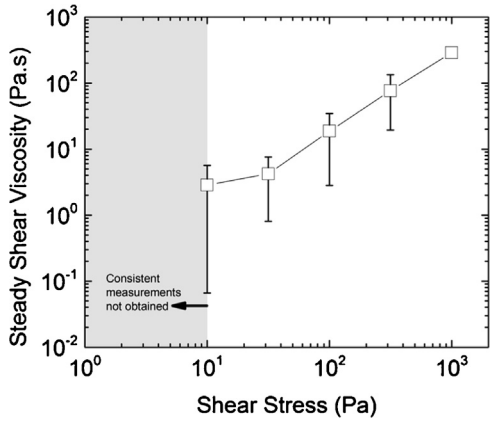

Fig. 7. Shear thickening in steady shear of the alumina paste with 0.2 wt% PVA binder. Inconclusive measurements were obtained from 1 to 10 Pa and shear thickening behavior was observed from 10 to 1000 Pa.

was observed as the steady state viscosity increased by a factor of 100. Although the material displayed shear thickening, it was unclear how important this was to enabling bead processing.

We conjecture that the primary rheological requirement for vibration processing is to behave as a solid at low stress on the relevant timescales to retain shape and behave as a nonlinear plastic material exhibiting limited strain recovery at higher stress to enable formation into rounded shapes. A yield stress would characterize this transition, and the required/target yield stress would need to lie within a particular range, depending on processing conditions and desired final shape of the bead. If shear-thickening is relevant, it may serve the secondary role of limiting the deformation of the paste during the largest impacts during processing. This may reduce the statistical variability of strains induced by vibration impacts and result in smoother beads. Here we have characterized what rheology is *sufficient* for processing, for the 0.2 wt% PVA formulation. The minimum rheological requirements, such as range of yield stress and presence of shear thickening, are beyond the scope of this work but could be tested by formulating a range of samples with deliberately different rheology.

3.5. Calcination and sintering of beads

Thermal analysis for calcination and sintering of the beads were conducted: First, TGA results confirmed that there was an initial ~9% weight loss decrease at 100 °C corresponding to the evolution of H_2O. This large amount of mass loss was due to the entrapped water within the outer dry shell of the green body. A ~2% at 425 °C mass loss was also observed, which corresponded to the burnout of the binder, dispersant, and any other organics (Fig. 8). The calcination was carried out at 700 °C for 1 h to complete decomposition of all volatile matter [43]. A slow calcination rate of 0.5 °C/min during calcination prevented thermal shock when the evaporation of the volatile matter occurred [43].

During sintering, the ramp-up rate was increased to 5 °C/min and the samples were sintered at various temperatures from 1400 °C to 1650 °C with increments of 50 °C to induce densification. The samples sintered at 1400 °C/4 h gave a density of 3.25 + 0.14 g/cm^3, but when the samples were sintered at 1650 °C/4 h, the density was 3.78 + 0.06 g/cm^3. There was a 14% increase in density when the temperature was incremented by 250 °C. To visually corroborate these results, the micrographs using SEM (Fig. 9(a)) reveal the porosity network of samples sintered at 1400 °C/4 h. Moreover, when looking at the average grain size of the samples sintered 1400 °C/4 h, two different features in the microstructure were observed: large agglomeration of grains (~20 μm in size) and small grains ranging between 1 and 3 μm

Table 2
Properties of alumina-sintered beads as a function of sintering temperature.

Sintering conditions	Bulk density (g/cm^3)	Theoretical density (%)	Bead diameter (mm)	Compressive load (N)
1400 °C/4 h	3.25 ± 0.14	83.4	8.50 ± 0.10	1122 ± 240
1450 °C/4 h	3.31 ± 0.15	84.9	8.50 ± 0.08	1712 ± 300
1500 °C/4 h	3.49 ± 0.14	89.4	8.50 ± 0.06	2161 ± 315
1550 °C/4 h	3.60 ± 0.08	92.3	8.50 ± 0.08	2716 ± 79
1600 °C/4 h	3.67 ± 0.07	94.1	8.50 ± 0.07	3948 ± 13
1650 °C/4 h	3.78 ± 0.06	97.0	8.50 ± 0.08	3954 ± 93

in size with a dense network of porosity (Fig. 9(b)). In the opposite case, where the samples were sintered at 1650 °C for 4 h, the microstructure revealed large grains ($x > 20$ μm in size) and a few large pores with ~15 μm in size.

3.6. Characterization of the alumina beads

The samples (five beads were measured and tested per condition) sintered at 1650 °C for 4 h had a compressive load strength of 3954 + 93 N, which was 71.6% higher than the samples sintered at 1400 °C/4 h. Table 2 summarizes breaking force, density, and bead diameters of tested samples.

The comminution results as a function of milling time provided more information (i.e. mass and diameter wear rate) on the performance of the alumina beads. Fig. 10 shows the bead diameter reduction and bead weight loss due to the milling of the beads. The

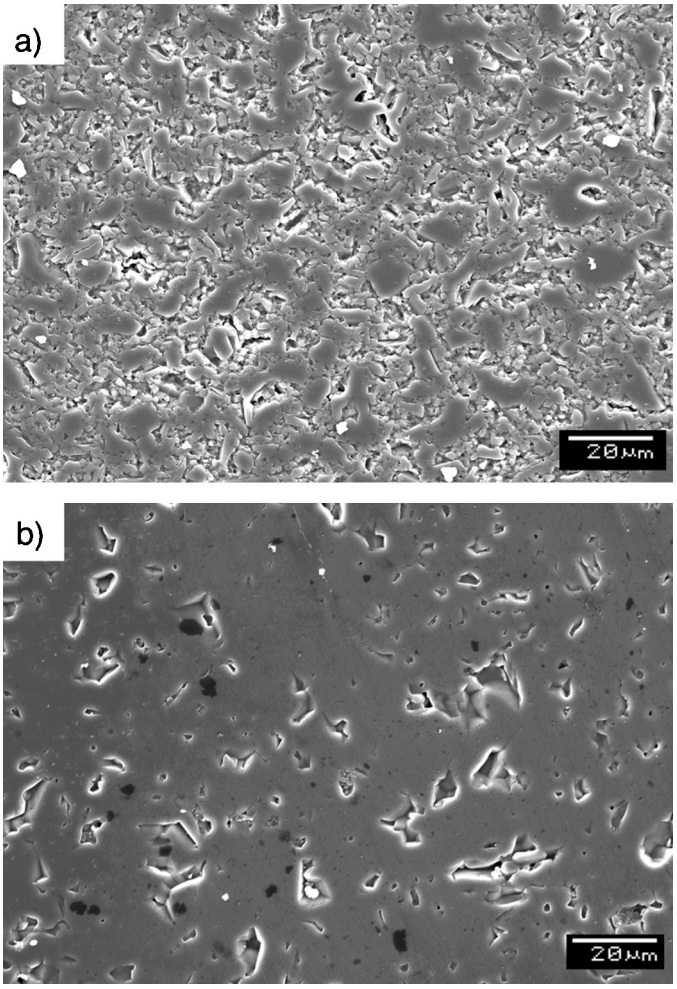

Fig. 9. SEM micrographs of the microstructure of alumina beads sintered for 4 h at (a) 1400 °C and (b) 1650 °C.

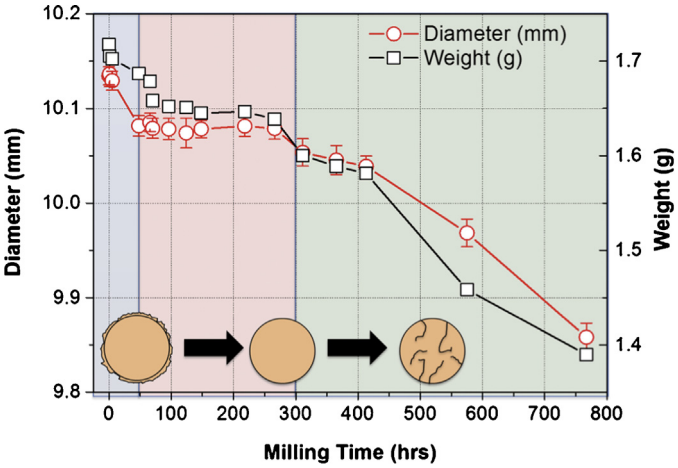

Fig. 10. Diameter and weight profiles of the alumina beads as a function of milling time, with the first (0–50 h), second (50–300 h), and third (300–800 h) stages of the bead evolution over milling time.

slopes in Fig. 10 are the diameter $\frac{d(m_b)}{d(t)}$ and mass $\frac{d(m_b)}{d(t)}$ wear rate from Eqs. (1) and (2).

In addition, Fig. 10 shows the three different stages of the alumina beads when they were exposed to longer milling time at a fixed 220 rpm. During the first stage, the rotating motion refined the surface of the beads; this step was considered as a refinement step to improve the finishing of the beads. The first stage occurred within the first 50 h of milling time and the average bead diameter was reduced by 0.7%. During the second stage, the average bead diameter remained constant without wear/erosion. The second stage happened between 50–300 h of milling time. The third stage occurred between 300 to 750 h of milling time; beads at this point experienced excessive material loss that resulted in the misshaping or fracturing of the alumina beads, similar observation was obtained in the literature [44]. Knowing the slopes of each plot allowed calculation of the mass (K_m) and diameter wear (K_d) rate constants for the alumina beads. Fig. 11(a) and (b) shows the mass and diameter rate constants calculated using Eqs. (1) and (2).

As the final characterization step, the eccentricity using Eq. (3) was calculated in the *xy*, *xz*, and *yz* planes. The data was divided into four groups based on the bead diameter. It was found that in all the planes for the four diameter groups, the eccentricity was below 0.07. Having an eccentricity below 0.07 indicates that the alumina beads could be produced by the vibration method, which are spherical (Fig. 12). In addition, Table 3 shows the distribution of the sphere-like type of beads measured.

Table 3
Selection of the type of ellipsoid for the alumina beads based on their radius in the xy, xz, and yz planes.

Tri-axial or scalene ellipsoid ($a > b > c$)	Oblate ellipsoid ($a = b > c$)	Prolate ellipsoid ($a = b < c$)	Sphere ($a = b = c$)
53.6%	25.0%	25.4%	0

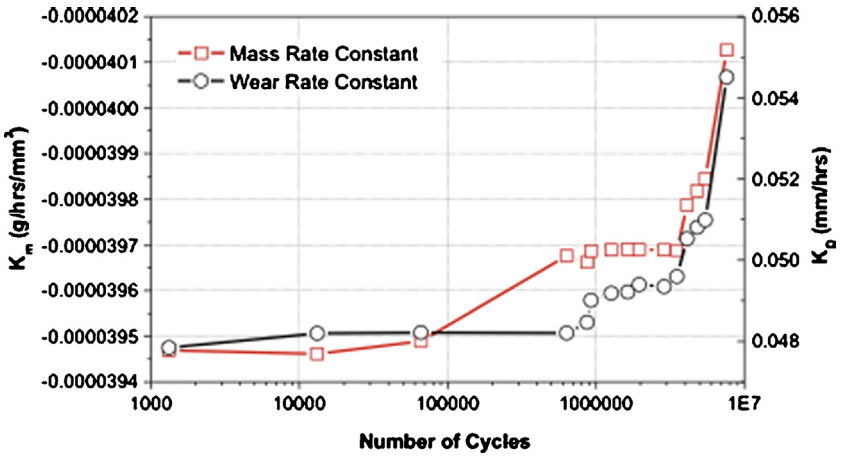

Fig. 11. The mass and diameter wear rate contact as a function of rotating cycles for alumina beads sintered at 1650 °C/4 h.

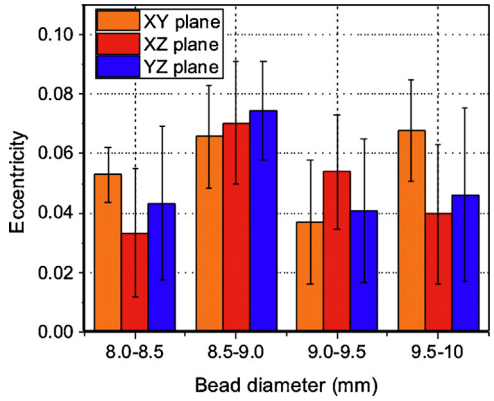

Fig. 12. Eccentricity in the *xy*, *xz*, *yz* planes for alumina beads sintered at 1650 °C for hours.

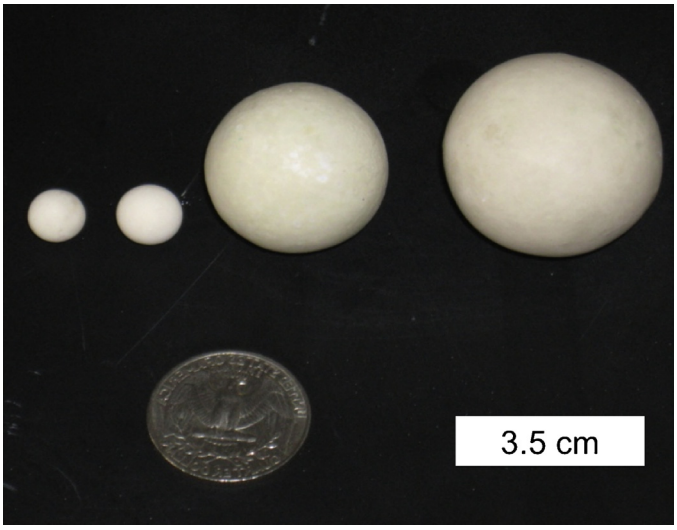

Fig. 13. Alumina beads sintered at 1650 °C for 4 h.

4. Conclusion

The vibration method proved to be effective in producing alumina beads having tailorable size (Fig. 13) and shape (i.e. oblate, prolate, and tri-axial ellipsoid). The best slurry composition to make alumina beads was with 0.2 wt% with a PVA binder. After the removal of water during the dehydration step, the composition changed to a workable paste with ~9 wt% water content. In addition, characterization of the alumina paste rheology indicated a viscoelastic solid at low stress (<2 Pa) with nonlinear softening upon the application of larger stress or strain. In the linear viscoelastic regime of small strains, the elastic storage modulus, G', always dominated the viscous loss modulus, G'', and no crossover frequency was observed. Furthermore, it was found that the frequency of impact (60 rad/s) fell within the tested range of the alumina paste. Moerover for shear stresses of 10 to 100 Pa, the nonlinear response was predominantly plastic as there was little recovery of the accumulated strain. For stresses in the range of 10 to 1000 Pa, the maximum recovery compliance was always less than 1%. Based on the thermal treatment process, the optimum conditions were 700 °C/1 h for calcination and 1650 °C/4 h for sintering where the density was 97% of theoretical value and the load of the alumina beads were ~3954 + 93 N. Furthermore, the refinement step provided more insight into the mechanical performance of the alumina beads. The three stages under longer milling times reveal that during the first 50 h, the bead diameter was reduced by 0.7%; during the second stage, the diameter remained constant; and during the third stage the alumina bead either fractured or became misshapen. Thus a processing method for making ceramic beads larger than 5 mm in diameter has been developed.

Acknowledgments

This work was funded by the Army Research Office (ARO), the DoD Multi University Research Initiative (MURI) Program through Dr. David Stepp under grant No. W911NF-09-1-0436. The authors acknowledge the National Science Foundation Graduate Research Fellowship Program (NSF-GRFP) under grant No. NSF DGE 11-44245 for their support during graduate school studies. Some of the experiments in this paper were carried out in the Frederick Seitz Materials Research Laboratory Central Facilities, University of Illinois at Urbana-Champaign, which are partially supported by the U.S. Department of Energy under grants DE-FG02-07-ER46453 and DE-FG02-07-ER46471. Rheological studies were conducted at the Ewoldt Research Labs at the University of Illinois. In addition, the authors acknowledge Mr. Benjamin Walusiak and Mr. Samuel Hayes for helping to with the setup of some of the experiments presented in this paper. Also, the authors acknowledge Dr. Pathikumar Sellappan and Mr. Kevin Seymour for providing recommendations to improve the quality of the paper.

References

[1] H. Hertz, On the contact of elastic solids, J. Reine Anges 92 (1881) 156–171.
[2] M. Job, S. Adam, S. Surajit, How Hertzian solitary waves interact with boundary in a 1D granular medium, Phys. Rev. Lett. 94 (2005) 178002.
[3] C. Daraio, V. Nesterenko, E.B. Herbold, S. Jin, Tunability of solitary wave properties in one-dimensional strongly nonlinear phononic crystals, Phys. Rev. E: Stat. Nonlinear Soft Matter Phys. 73 (2006) 026610.
[4] Job M, Santibanez F, Tapia F. Nonlinear waves in Hertzian granular chains: effects of inertial and stiffness Heerogeneities. Proceedings of the International Congress on Ultrasonics: 1–5.
[5] V. Nesterenko, Solitary waves in discrete media with anomalous compressibility and similar to "sonic vacuum", J. Phys. IV France 04 (1994) C8-729.
[6] E.F. Coste, S. Fauve, Solitary waves in a chain of beads under Hertz contact, J. Phys. Rev. E 56 (1997) 5.
[7] T. On, Experimental study of the development of plastic waves in one-dimensional granular media, Vol. Master of Science in Aerospace Engineering, Department of Aerospace Engineering, University of Illinois at Urbana-Champaign, 2011, pp. 1–63.
[8] T. On, L.A. LaVigne, J. Lambros, Development of plastic nonlinear waves in one-dimensional ductile granular chains under impact loading, Mech. Mater. 68 (2014) 29–37.
[9] C. Daraio, V. Nesterenko, Strongly nonlinear wave dynamics in a chain of polymer coated beads, Phys. Rev. E: Stat. Nonlinear Soft Matter Phys. 73 (2006) 026612.
[10] A.C. Hulst, T.K. Van't Riet, J.M. Westerbeek, A new technique for the production of immobilized biocatalyst in large quantities, Biotechnol. Bioeng. 27 (1985) 870–876.
[11] H.L. Walker, W.J. Connick, Sodium alginate for production and formulation of mycoherbicides, Weed Sci. 31 (1983) 333–338.
[12] C.J. Espinoza Santos, T.S. Wei, B. Cho, W.M. Kriven, A forming technique to produce spherical ceramic beads using sodium alginate as a precursor binder phase, J. Am. Ceram. Soc. 96 (11) (2013) 3379–3388.
[13] J.R. Fair, D.E. Steinmeyer, W.R. Penny, J.A. Brink, Liquid-gas systems, in: Chemical Engineer's Handbook, McGraw-Hill: The Univeristy of California, 1973.
[14] J.S. Klein, J. Vorlop, Pore size and properties of spherical ca-alginate biocatalysts, Appl. Microbiol. Biotechnol. 18 (1983) 86–91.
[15] U. Matulovic, D. Rasch, F. Wagne, New equipment for the scaled up production of small spherical biocatalysts, Biotechnol. Lett. 8 (7) (1986) 485–490.
[16] Vlach TJ, Yaroshenko V, Pujar VV. Method of forming ceramic beads. pp. 7. in, Vol. US 6797203 B2. CerCo LLC, United States, 2004.
[17] A. Bégin, F. Castaigne, J. Goulet, Production of alginate beads by a rotative atomizer, Biotechnol. Tech. 5 (1991) 459–464.
[18] B. Bugarski, Q. Li, M. Goosen, D. Poncelet, R.J. Neufeld, G. Vunjak, Electrostatic droplet generation: mechanism of polymer droplet formation, AIChE J. 40 (1994) 1026–1031.
[19] S. Romo, C. Pérez-Martínez, The use of immobilization in alginate beads for long-term storage of pseudanabena galeata (cyanobacteria) in the laboratory, J. Phycol. 33 (1997) 1073–1076.
[20] P.W. Walsh, F.V. Isdell, S.M. Noone, M.G. O'Donovan, D.M. Malone, Growth patterns of saccharomyces cerevisiae microcolonies in alginate and carrageenan gel particles: effect of physical and chemical properties of gels, Enzyme Microb. Technol. 18 (1996) 366–372.
[21] Y. Monakhova, P. Agulhon, F. Quignard, N. Tanchoux, D. Tichit, New mixed lanthanum- and alkaline-earth cation-containing basic catalysts obtained by an alginate route, Catal. Today 189 (1) (2012) 28–34.
[22] T. Nozaki, T. Arima, K. Idemitsu, J. Inagaki, Synthesis of zirconia sphere particles based on gelation of sodium alginate, J. Nucl. Mater. 412 (2011) 184–219.
[23] S. Abramson, C. Meiller, P. Beaunier, V. Dupuis, L. Perrigaud, A. Bee, V. Cabuil, Highly porous and monodisperse magnetic silica beads prepared by a green templating method, J. Mater. Chem. 20 (2010) 4916–4924.
[24] K. Teraoka, K. Kato, Production of alpha-tcp ceramic precision spheres for mosaic-like ceramics fabrication use, Bioceram. Dev. Appl. J. 1 (2010) 1–3.
[25] J. Yang, J. Yu, Y. Huang, Recent developments in gelcasting of ceramics, J. Eur. Ceram. Soc. 31 (2011) 2569–2591.
[26] P. Garcia-Perez, C. Pagnoux, A. Pringuet, A. Videcoq, J.F. Baumard, Agglomeration of alumina submicronparticles by silica nanoparticles: application to processing spheres by colloidal route, J. Colloid Interface Sci. 313 (2007) 527–536.
[27] N. Dilsiz, G. Akovalı, Study of sol–gel processing for fabrication of low density alumina microspheres, Mater. Sci. Eng., A 332 (2002) 91–96.
[28] G.V. Franks, B.V. Velamakanni, F.F. Lange, Vibra Forming and in situ flocculation of consolidated, coagulated, alumina Slurries, J. Am. Ceram. Soc. 78 (1995) 1324–1328.
[29] Velamakanni BV, Lange FF. Method for preparation of dense ceramic products. in United States Patent, Patent US005188780A. Edited by The Regents of the University of California, United States, 1991.
[30] B.V. Velamakanni, J.C. Chang, F.F. Lange, D.S. Pearson, New method for efficient colloidal particle packing via modulation of repulsive lubricating hydration forces, Langmuir 6 (1990) 1323–1325.
[31] P.E. Luther, T.M. Kramer, F.F. Lange, D.S. Pearson, Development of short-range repulsive potentials in aqueous, silicon nitride slurries, J. Am. Ceram. Soc. 77 (1994) 1047–1051.
[32] J. Yu, J. Yang, Y. Huang, The transformation mechanism from suspension to green body and the development of colloidal forming, Ceram. Int. 37 (2011) 1435–1451.
[33] Y.P. Pivinskii, Refractory concretes of new generation. Vibrorheology, vibration methods of compacting and forming, Refractories 35 (1994) 211–220.
[34] J.R. Evans, Seventy ways to make ceramics, J. Eur. Ceram. Soc. 28 (2008) 1421–1432.
[35] J. Requena, R.J. Moreno, J.S. Moya, Alumina and alumina/zirconia multilayer composites obtained by slip casting, J. Am. Ceram. Soc. 72 (1989) 1511–1513.
[36] Buck G.M. and Vasquez P. Ceramic slip casting technique in Google Patents 1993.
[37] W.D. Kingery, JH.K. Bowen, D.R. Uhlmann, Introduction to Ceramics, 2nd ed., John Wiley & Sons, New York, NY, 1976.
[38] ASTM International, Standard Test Method for Water Absorption, Bulk Density, Apparent Porosity, and Apparent Specific Gravity of Fired Whiteware Products, ASTM International, West Conshohocken, 2006, pp. 1–2, PA 1.
[39] M. Schwedes, Comminution of ceramics in stirred media mills and wear of grinding beads, J. Powder Technol. (1999) 374–381.
[40] W.B. Zhong, Z. Lianmeng, F. Fang, H. Xiaoyi, Prediction and experimental testing of spherical milling media wear rate, Mater. Trans. 46 (2005) 2036–2040.
[41] H. Wadell, Volume, shape, and roundness of quartz particles, J. Geol. 43 (1935) 250–280.
[42] H.A. Barners, Shear Thickening ("dilatancy") in suspensions of nonaggregating solid particles dispersed in newtonian liquids, J. Rheol. 329 (1989) 329–366.
[43] S.J. Lee, E.A. Benson, W.M. Kriven, Preparation of portland cement components by poly(vinyl alcohol) solution polymerization, J. Am. Ceram. Soc. 82 (1999) 2049–2055.
[44] M. Becker, J. Schwedes, Comminution of ceramics in stirred media mills and wear of grinding beads, Powder Technol. 105 (1–3) (1999) 374–381.